NJC

ROYAL SOCIETY OF CHEMISTRY

PAPER

View Article Online
View Journal | View Issue

Cite this: *New J. Chem.*, 2025, 49, 10538

Tuning the electronic structure of BODIPY-coumarin ratiometric fluorescent sensors for accurate microviscosity monitoring applications†‡

Enrique Ordaz-Romero, [a] Angela Y. Díaz-Flores, [a] Sandra M. Rojas-Montoya, *[a] Luis Blancarte-Carrazco, [a] Margarita Romero-Ávila, [a] Pablo Labra-Vázquez, *[a] Rosa Santillan [b] and Norberto Farfán *[a]

Received 27th February 2025,
Accepted 29th May 2025

DOI: 10.1039/d5nj00899a

rsc.li/njc

Fluorescent molecular rotors (FMRs) have emerged as versatile tools for assessing microviscosity in biological and physicochemical environments. This study presents the design, synthesis, and characterization of two novel ratiometric viscosity sensors based on BODIPY-coumarin derivatives, in which the chromophores are electronically isolated by an ester bridge. This structural feature aims to mitigate polarity-dependent effects and optimize their ratiometric performance. The synthesis was carried out through a multistep approach, including microwave-assisted esterification, achieving high yields. Structural characterization, based on single-crystal X-ray diffraction and DFT calculations, confirmed the electronic isolation of the chromophores, while photophysical studies revealed polarity-independent emission from the BODIPY fragment. Both sensors exhibited high sensitivity to viscosity variations over a broad range in DMSO/glycerol mixtures. These findings highlight the potential of these FMRs as advanced tools for microenvironment studies, providing a promising platform for future applications in biochemistry and materials science.

Introduction

In recent decades the development of optical sensors has advanced considerably, driven by the need for more precise and versatile tools for analyzing biological systems and complex materials such as liquid crystals,[1] polymeric gels,[2] emulsions,[3] and micelles,[4] among others. The optimization of fluorophores and detection strategies has enhanced the sensitivity and selectivity of these sensors, expanding their application to the study of microenvironments and dynamic processes at the molecular level. Among these tools, ratiometric sensors have proven highly useful due to their ability to provide a highly accurate and reliable measurement by minimizing the effects of sensor concentration and experimental conditions. These sensors, based on the ratio of optical signals from different submolecular fragments, have found applications in areas such as bioimaging,[5] monitoring cellular processes,[6] and analyzing physicochemical properties in biological media.[7]

One of the most relevant parameters that can be detected using ratiometric sensors is microviscosity, which along with molecular crowding, is a critical factor in the biological environment for proper cellular function. Subtle alterations in these parameters have been linked to various pathologies, including diabetes,[8] malaria,[9] cancer,[10] and neurodegenerative diseases such as Parkinson's,[11] Huntington's,[12] and Alzheimer's.[13] In this context, ratiometric sensors based in fluorescent molecular rotors (FMRs) have emerged as key tools for addressing microviscosity in biological contexts, with bichromophoric ratiometric FMRs, where only one of the chromophores is viscosity-dependent, lying among the most studied types of ratiometric sensors[14] due to several advantages of these molecular devices.[15] Among other characteristics, an ideal ratiometric sensor should exhibit both high sensitivity and selectivity to small microviscosity fluctuations, remaining unaltered upon changes in other physicochemical parameters of the surrounding media.

Among the fluorophores used to build ratiometric sensors, coumarins and BODIPYs (boron-dipyrromethenes) have

[a] *Facultad de Química, Departamento de Química Orgánica, Universidad Nacional Autónoma de México, Ciudad Universitaria, 04510 Ciudad de México, Mexico. E-mail: sandmarcela@gmail.com, pab.labra@gmail.com, norberto.farfan@gmail.com, nfarfan@unam.mx*

[b] *Departamento de Química, Centro de Investigación y de Estudios Avanzados del IPN, Apdo. Postal 14-740, 07000, Ciudad de México, Mexico*

† Heartwarmingly dedicated to Dr Pascal Lacroix (LCC-CNRS) in the occasion of his retirement.

‡ Electronic supplementary information (ESI) available: Copies of NMR and HRMS spectra and computational details. CCDC 2424050. For ESI and crystallographic data in CIF or other electronic format see DOI: https://doi.org/10.1039/d5nj00899a

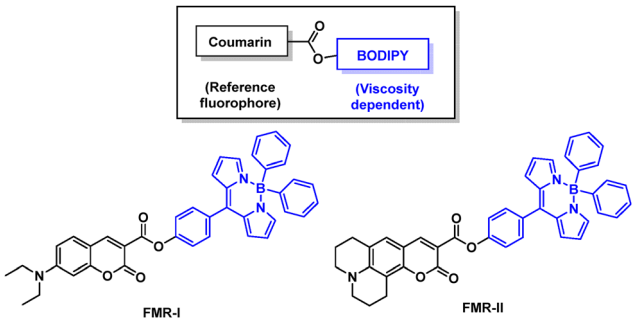

Scheme 1 Molecular structure of the investigated fluorescent molecular rotors (FMRs).

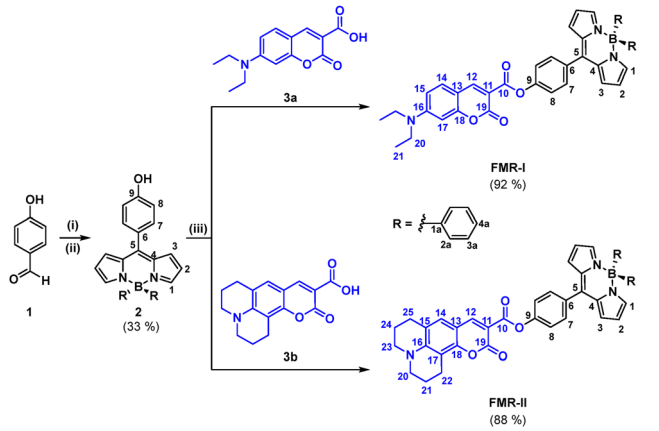

Scheme 2 Synthesis and numbering of fluorescent molecular rotors **FMR-I** and **FMR-II**. *Reagents and conditions*: (i) Pyrrole, TFA, DCM, rt; (ii) DDQ, diphenylborinic acid, THF, reflux; (iii) DCC, DMAP, DCM, microwave irradiation (100 W, 80 °C).

demonstrated exceptional versatility due to their exceptional properties such as high chemical stability[16–18] and efficient optical absorption and emission properties in the visible region.[19–21] Because of their well-separated emission, combining these two chromophores into a single molecule can enable the obtention of bichromophoric ratiometric FMRs. In a previous study by our research group, we reported on microviscosity sensors based on the conjugation of these two molecular scaffolds.[22] While the developed sensors turned out highly sensitive to changes in viscosity, with a ratiometric response over a broad viscosity range, both chromophores were conjugated, resulting in a high static dipolar moment and the emission from the BODIPY fragment being highly sensitive to polarity, as an analytical limitation of these FMRs.

In this work we explore an alternative way to link the BODIPY and coumarin chromophores, aiming at electronically isolating them from each other and thus obtaining polarity-independent viscosity sensors. The molecular structure of the investigated compounds is shown in Scheme 1, where the viscosity-sensitive BODIPY fluorophore is attached to two different coumarin derivatives, employed as viscosity-independent reference fluorophores. An ester bridge is used to avoid conjugation between both submolecular fragments. The paper is organized as follows: first we present the synthesis and characterization of the molecules, followed by a structural analysis with support from single-crystal X-ray diffraction (SXRD) and DFT computations. Then, we discuss the optical absorption and emission properties and the viscosity sensing of the fluorophores. We end by summarizing our findings and highlighting the strengths and limitations of the developed sensors.

Results and discussion

Synthesis and characterization

The synthetic route towards the target compounds is shown in Scheme 2. The synthesis started by the preparation of BODIPY derivative **2** bearing a coordinated BPh_2 moiety and a 4-hydroxyphenyl group at the *meso* position. This compound was conveniently accessed following the two-step procedure reported by our group for structurally-related fluorophores.[23] It involved the condensation of 4-hydroxybenzaldehyde (**1**) with pyrrole in acidic media to give the corresponding *meso*-(4-hydroxyphenyl)-dipyrromethane,[24] which was isolated and further oxidized with 2,3-dichloro-5,6-dicyano-1,4-benzoquinone (DDQ) and coordinated with diphenylborinic acid to give BODIPY **2** in a moderate yield. Then, BODIPY 2 was esterified using dicyclohexylcarbodiimide (DCC) as coupling agent and carboxy-functionalized coumarin derivatives **3a-b** as coupling partners, yielding the target fluorophores **FMR-I** and **FMR-II** in excellent yields. It should be noted that the final synthetic step was challenging, forcing us to optimize the reaction conditions with both conventional heating and microwave irradiation being explored.

The identity of BODIPY 2 and of the target fluorophores (**FMR-I** and **FMR-II**) was corroborated employing a combination of spectroscopic and spectrometric techniques, featuring multinuclear ($^1H/^{13}C/^{11}B$) NMR, FT-IR (ATR) and mass spectrometry analyses. Furthermore, we were able to grow crystals of **FMR-I** that were analyzed by single-crystal X-ray diffraction (SXRD), with the crystal structure corroborating the identity of the fluorophore, as discussed in detail in the following section. An unambiguous assignment of the NMR spectra of these compounds was carried out employing a combination of homonuclear ($^1H/^1H$) COSY and heteronuclear ($^1H/^{13}C$) HSQC/HMBC 2D-NMR experiments. Ambiguity found in the assignment of some of the ^{13}C-NMR signals was further circumvented using Gauge-invariant atomic orbital (GIAO) computations[25,26] of isotropic magnetic shieldings on DFT-optimized conformations of these molecules.

These NMR studies offered a first glance into the ground-state electronic structure of the target fluorophores, for which our design strategy required the coumarin and BODIPY submolecular fragments electronically isolated from each other. As exemplified with **FMR-I** in Fig. 1, upon esterification the chemical shift for most of the ^1H- and ^{13}C-NMR signals remained relatively unchanged, with only hydrogens H-7 and H-8 resonating at higher frequencies when compared with their homologue signals in BODIPY **2**. Contrary to our above

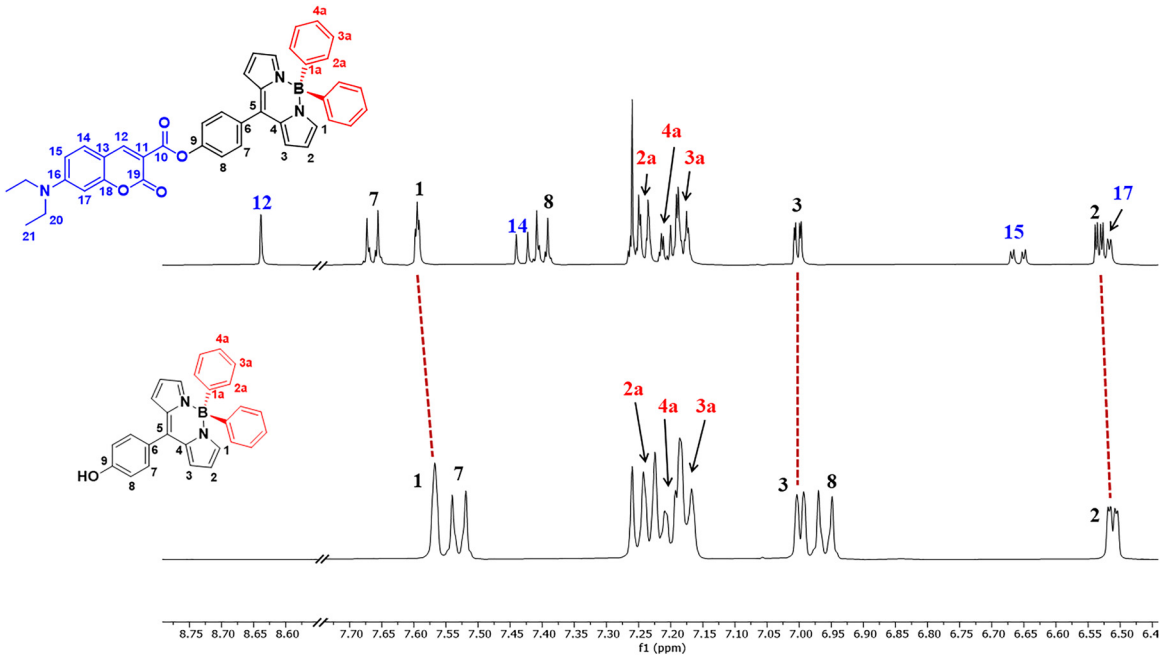

Fig. 1 Comparison of the aromatic region of the ^{1}H-NMR spectra for **FMR-I** (top) and BODIPY **2** (bottom), showcasing the limited electronic influence of the coumarin fragment on the BODIPY core, as evidenced by the relatively unaltered chemical shifts for hydrogens H-1 to H-3. Spectra were recorded at 298 K in $CDCl_3$ in a 500 MHz spectrophotometer.

expectations, the deshielding of these hydrogens suggests an electron-withdrawing effect introduced by the carboxy-coumarin fragment on the BODIPY fluorophore. The effect, however, is limited to the phenyl ring and arises due to the fact that the –OH group in BODIPY **2** (an electron donor) becomes part of an ester group (an electron withdrawing group) in **FMR-I** and **FMR-II**. Furthermore, signals corresponding to hydrogens H-1 to H-3, belonging to the BODIPY core remained unaltered, indicating the localized nature of this effect. These observations gratifyingly confirmed a ground-state electronic structure for **FMR-I** and **FMR-II** where both the coumarin and BODIPY submolecular fragments are electronically isolated from each other thanks to their association through the ester linker, which hampers electronic delocalization. As detailed later in the manuscript (*vide infra*), optical absorption studies and TD-DFT computations offered additional concurring evidence on the absence of electronic transitions between these fragments in the ground state, thus ratifying our molecular engineering approach for these molecules.

Structural analysis

Having discussed the synthesis and characterization of the target fluorophores, here we will present a structural analysis of these molecules with support from single-crystal X-ray diffraction (SXRD) and DFT computations. Crystallization experiments for both fluorophores were conducted by slow evaporation of saturated solutions of the analytes in various solvents. These experiments proved successful for **FMR-I**, which yielded orange plates when crystallized from chloroform. Contrarywise, **FMR-II** produced either amorphous or poorly crystalline samples, thus precluding SXRD studies on this compound.

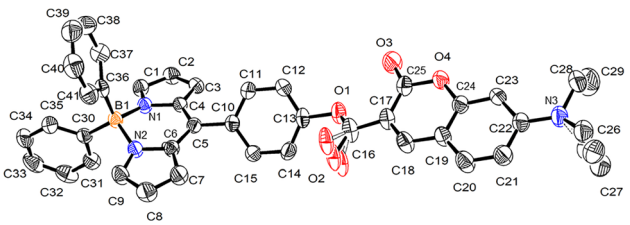

Fig. 2 Asymmetric unit for fluorophore **FMR-I** with thermal ellipsoids drawn at 50% probability. Hydrogen atoms were omitted for clarity. Selected bond lengths [Å] and angles [°]: B1–N1 1.571(3), B1–N2 1.574(3), B1–C30 1.614(3), B1–C36 1.623(3), N1–B1–N2 102.67(15), N1–B1–C30 109.44(17), N1–B1–C36 109.66(18), N2–B1–C30 111.15(18), N2–B1–C36 110.16(17).

The crystal structure of **FMR-I** was solved in the triclinic $P\bar{1}$ spacegroup. The molecule crystallized solventless with two molecules of the fluorophore per unit cell (Z = 2), related to each other by inversion symmetry. The asymmetric unit is depicted in Fig. 2, while the associated crystallographic data is included as ESI‡ (Table S2). As further detailed in the ESI‡ (Section S3), the crystal packing of **FMR-I** is dominated by the formation of symmetric dimeric self-assemblies where the bulky phenyl groups attached to the boron atom inhibit the stacking of adjacent BODIPY fragments, an interesting feature that can explain the emissive properties that were qualitatively observed for **FMR-I** and **FMR-II**, that parallels previous studies where the introduction of bulky substituents on BODIPY fluorophores has been exploited for obtaining solid-state emissive BODIPY derivatives.[27]

The asymmetric unit of **FMR-I** shows disorder in the carbonyl of the ester bridge and in one of the alkyl chains of the

diethylamino group, potentially arising from thermal vibrations, considering that the data was collected at 293 K. The crystallographic conformation shows an overall non-planarity due to the nonplanar connection between the phenyl-BODIPY fragment and the ester bridge, as evidenced by a significant C14–C13–O1–C16 torsion angle of 56.3°. While the fused bicyclic system of the coumarin fragment is planar, the BODIPY fragment displays a 48.98° (C4–C5–C10–C11) torsion angle between the phenyl ring and the dipyrrin core, associated with steric hindrance.

More remarkably, the boron atom in the crystal structure of **FMR-I** is slightly shifted above the dipyrrin plane, an interesting feature that is not observed for BODIPY derivatives with fluorine substitution at the boron.[28–30] This is accompanied by a distorted tetrahedral geometry for the boron atom with a N1–B1–N2 angle of 102.67°. The two phenyl groups attached to the boron atom show significantly different orientations with respect to the dipyrrin core, with 37.32° (C4–C5–C6–C36) and 4.76° (C4–C5–B1–C30) dihedral angles for the phenyl rings 'above' and 'below' the dipyrrin plane, respectively. Although these observations follow a recent report on structurally-related BODIPY fluorophores,[31] no explanation for these interesting features has been informed.

In order to understand the origins of the structural features observed in the crystallographic structure of **FMR-I**, DFT computations were performed at the M06-2X/6-31+G(d,p) level of theory in vacuum following two approaches. In the first approach, hydrogens and disordered heavier atoms were freely optimized, with the resulting 'relaxed' geometry consequently closely resembling the crystallographic conformation. In the second approach, the molecule was optimized without imposing any constraints, thus precluding any effects from the crystal packing.

The obtained geometries are illustrated in Fig. 3(a), with the most significant difference being a co-planar configuration between the BODIPY and coumarin fragments for the freely-optimized gas-phase conformer. The deviation from planarity for the SXRD conformer makes it *ca.* 8.3 kcal mol^{-1} less favorable than the gas-phase conformation, as an energy difference easily overcome by the various supramolecular interactions stablished by the fluorophore in the solid state. It is important to remark that asides this deviation, both the SXRD and the gas-phase conformers are strikingly similar regarding the conformation around the boron center, which displayed negligible differences in bond distances and angles for its distorted tetrahedral geometry. The sole significant difference in this regard is that the phenyl ring lying 'above' the dipyrrin plane is rotated towards a pyrrole ring in the gas-phase conformer while it heads towards the center of the BODIPY core in the crystallographic conformation.

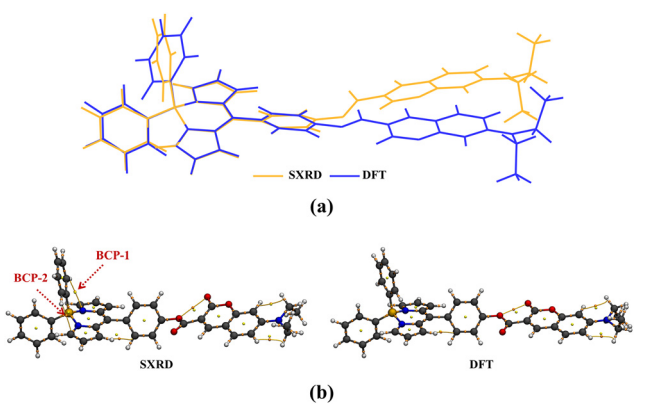

Fig. 3 (a) Overlay of DFT-computed conformations for **FMR-I** (M06-2X/6-31+G** in vacuum), with a 'relaxed' single-crystal X-ray diffraction (SXRD) conformation in orange (hydrogen and disordered heavier atoms optimized) and a freely-optimized conformation in blue. (b) Molecular graphs for both conformers with bond critical points (3, −1) in orange and ring critical points (3, +1) in yellow.

To further unveil the origins of these structural features, the bonding in both conformers was analyzed through topological analyses of the electron charge density within the framework of the quantum theory of atoms-in-molecules (QTAIM), a robust methodology for identifying and characterizing covalent and non-covalent interactions in molecular systems.[32–34]

As depicted in Fig. 3(b), the molecular graphs for both conformers are very similar, with the most significant difference being that in the SXRD conformer the phenyl ring 'above' the BODIPY plane stablishes C37–H37···N1 and C41–H41···π non-covalent interactions. Due to their poor directionalities and long D–H···A distances, these interactions can be considered as weak nonclassical hydrogen bonding interactions.[35,36] Indeed, the interaction energies (E_{int}), as evaluated from the potential energy density, $V(r)$, at the bond critical points (BCP-1 and BCP-2, respectively) using the Espinosa–Molins–Lecomte relationship[37] leads to E_{int} values of −8.37 and −7.52 kcal mol^{-1}, respectively. Interestingly, due to the different orientation of the phenyl ring, these stabilizing interactions are absent in the gas phase conformer, which can be ascribed to a preference towards a more efficient orbital overlap of the phenyl ring with the π-system of the dipyrrin core. Because of the net positive charge delocalized within the dipyrrin core, this alternative interaction can be expected to be highly stabilizing, as it can help further delocalize the positive charge through hyperconjugative interactions.

It is important to remark that although as mentioned above we were unable to obtain crystals of **FMR-II** of enough quality to be structurally characterized by SXRD, due to the lack of conjugation between the BODIPY and coumarin submolecular fragments, the conclusions from the above structural analysis on **FMR-I** can be largely extrapolated to **FMR-II**. In fact, as shown in ESI,‡ Fig. S1, the freely-optimized molecular structure and the corresponding molecular graph for **FMR-II** showed largely equivalent features to those found for **FMR-I** in the gas phase, evidencing the structural similarity between both fluorophores.

To summarize, in this section we presented a structural analysis of the target fluorophores with support from DFT computations and SXRD data in the case of **FMR-I**. These analyses evidenced a unique structural feature of the BODIPY fragment in these fluorophores when compared to structurally-related BODIPY fluorophores that bear fluorine substituents at

the boron instead of phenyl groups as in the present study. The presence of these phenyl substituents induces a displacement of the boron atom above the dipyrrin plane and an orientation of a phenyl group towards a pyrrole ring, an effect accounted to an enhancement of electron delocalization *via* hyperconjugation of the phenyl ring with the positively-charged dipyrrin core. As discussed in detail in the following section, TD-DFT computations in DMSO for both **FMR-I** and **FMR-II** provided further evidence of this effect, with a significant participation of the Ph_2B moiety as an electron donor in the electronic transitions associated with the optical spectra of these compounds, thus providing support for the proposed hyperconjugative donor role of the Ph_2B fragment.

Photophysical properties and TD-DFT computations

Following our structural analyses on the target fluorophores, here we will present an investigation of their optical absorption and emission properties with the dual aim of (a) understanding the nature of the electronic transitions involved in the optical absorption and emission spectra and (b) discussing the behavior of both fluorophores in different solvents, to evaluate their potential impact on the fluorescent viscosity sensing properties that are discussed in detail in the following section.

The photophysical properties of the target fluorophores were first studied in DMSO by UV-Vis spectroscopy and steady-state fluorescence spectroscopy. DMSO was chosen as low concentrations of this solvent typically display negligible toxicity,[38] and is therefore frequently employed in biological studies.

The absorption and emission spectra for the target fluorophores and the associated data are presented in Table 1 and Fig. 4(a). The corresponding data for the starting fluorophores (BODIPY **2** and coumarins **3a-b**) are included as ESI‡ (Fig. S17–S19 and Table S2). As can be seen, both **FMR-I** and **FMR-II** displayed similar absorption spectra, with two intense bands centered around λ = 500 and 431 (**FMR-I**)/451 (**FMR-II**) nm and a lower intensity band around λ = 350 nm. According to TD-DFT computations at the M06-2X/6-31+G(d,p) level in DMSO, in both fluorophores these bands are ascribed to the $S_0 \rightarrow S_1$, $S_0 \rightarrow S_2$ and $S_0 \rightarrow S_6$ transitions, respectively.

As depicted in the frontier orbital energy diagram presented in Fig. 4(b), none of these transitions involve electronic polarization between the coumarin and BODIPY fluorophores, in good agreement with the NMR analyses discussed previously, which also showed both fluorophores being electronically isolated in the ground state, thus providing support to the molecular design strategy for these FMRs. Further evidence of the electronic isolation of both fluorophores in **FMR-I** and **FMR-II** arise by comparing their UV-Vis spectra with those of the starting fluorophores (**2**, **3a-b**), with the spectra of the target fluorophores constituting roughly the sum of their starting materials.

The nature of the electronic transitions in the target fluorophores are strikingly similar in both compounds, with the $S_0 \rightarrow S_1$ and $S_0 \rightarrow S_2$ transitions representing local excitations within the BODIPY and coumarin fragments, respectively. A charge transfer character is observed in the case of the $S_0 \rightarrow S_2$ transition, as it involves electron density polarization from the amino-substituted phenyl ring towards the benzannulated lactone ring of the coumarin, as a consequence of the evident push–pull architecture of this submolecular fragment. Finally, the $S_0 \rightarrow S_6$ transition in both compounds is located at the BODIPY fragment and has a charge transfer character, where the positively-charged dipyrrin core acts as a strong electron withdrawing group and both the phenyl ring attached to the *meso*-position and the phenyl groups from the Ph_2B moiety act as electron donors. This interesting observation is in good agreement with our earlier structural discussions, where we proposed that the geometry of the Ph_2B moiety is stabilized by hyperconjugative interactions with the dipyrrin core.

The fluorescence spectra of **FMR-I** and **FMR-II** in DMSO, registered at λ_{exc} = 440 nm, depicted the presence of both the coumarin and the BODIPY fluorescent bands, centered around λ_{em} = 480 and 520 nm, respectively, with the coumarin band in **FMR-II** being more intense due to a significantly higher fluorescent quantum yield (Φ_F) of the parent carboxy-coumarin fluorophore in DMSO (**3b**, Φ_F = 0.737) when compared to its counterpart in **FMR-I** (**3a**, Φ_F = 0.098). It should be noted that the Φ_F values f**or FMR-I** and **FMR-II** are particularly low (2×10^{-4} and 4×10^{-4}, respectively), which can tentatively

Table 1 Experimental (10^{-5} M in DMSO) and computed (M06-2X/6-31+G**/PCM:DMSO) UV-Vis data and experimental fluorescence data (10^{-5} M in DMSO, λ_{exc} = 440 nm) for the target fluorophores

	UV-Vis	TD-DFT			Fluorescence	
	λ_{max} [nm] (ε [M^{-1} cm^{-1}])	λ_{max} [nm] (f) transition	CI expansion	Dominant character	λ_{em} [nm]	Φ_F
FMR-I	501 (46 700)	424 (0.410) $S_0 \rightarrow S_1$	97% $\chi_{168 \rightarrow 170}$	BODIPY → BODIPY	519, 480	2×10^{-4}
	431 (49 000)	367 (1.327) $S_0 \rightarrow S_2$	93% $\chi_{169 \rightarrow 171}$	Coumarin → Coumarin		
	346 (9700)	309 (0.144) $S_0 \rightarrow S_6$	27% $\chi_{162 \rightarrow 170}$ + 27% $\chi_{165 \rightarrow 170}$	Ph_{bridge}/Ph_2B → BODIPY		
FMR-II	500 (66 400)	424 (0.416) $S_0 \rightarrow S_1$	97% $\chi_{174 \rightarrow 176}$	BODIPY → BODIPY	516, 485	4×10^{-4}
	451 (74 000)	380 (1.177) $S_0 \rightarrow S_2$	96% $\chi_{175 \rightarrow 177}$	Coumarin → Coumarin		
	346 (9700)	309 (0.185) $S_0 \rightarrow S_6$	38% $\chi_{167 \rightarrow 176}$ + 31% $\chi_{170 \rightarrow 176}$	Ph_{bridge}/Ph_2B → BODIPY		

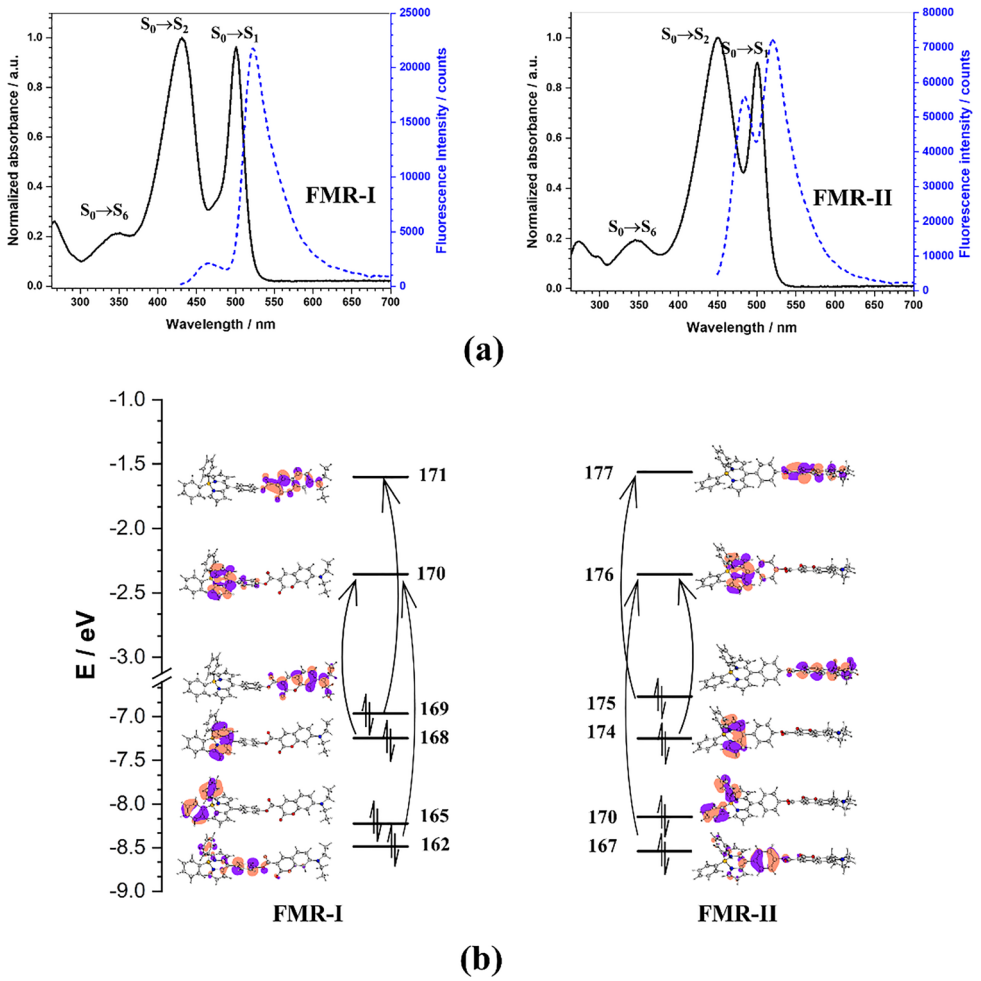

Fig. 4 (a) Optical absorption and emission spectra for **FMR-I** and **FMR-II** from 10^{-5} M solutions of the fluorophores in DMSO. Emission spectra were measured under excitation at λ_{exc} = 440 nm. (b) Dominant frontier orbitals involved in the $S_0 \rightarrow S_1$, $S_0 \rightarrow S_2$ and $S_0 \rightarrow S_6$ transitions for **FMR-I** (HOMO = 169) and **FMR-II** (HOMO = 175) at the M06-2X/6-31+G(d,p)/PCM:DMSO level of theory.

be accounted to photoinduced electron transfer (PET) processes occurring between the Ph_2B fragment and the dipyrrin core. Although further investigations to demonstrate this hypothesis lie outside the scope of the current work, the structural analyses presented in this paper clearly demonstrate the orbital overlap between these fragments, required for PET processes, which are well-known to compete efficiently with fluorescence,[39,40] as a reasonable explanation of the recurrent lower Φ_F values observed for Ph_2B BODIPYs when compared to their fluorine substituted counterparts.[31]

In any case, the clear observation of both the coumarin and BODIPY emissions, along with the electronical isolation of both fluorophores in the ground state constitute compelling evidence of the usefulness of **FMR-I** and **FMR-II** as ratiometric sensors.

As stated earlier in this manuscript, an analytical limitation of structurally-related coumarin-BODIPY ratiometric viscosity sensors reported previously by our research group,[22] was the significant influence of the solvent polarity in the emission from the BODIPY fragment. One of the main objectives of this work was to tackle this problematic by disrupting electronic conjugation between both fluorophores. To evaluate the extent to which the developed FMRs addressed this issue, we performed a solvatochromic study on the target compounds using solvents of varying polarity, with dielectric constants (ε) ranging from ε = 2.36 to 47.24 D.[41] The optical absorption spectra are presented in Fig. 5, gratifyingly displaying a negligible influence of solvent polarity in the optical absorption spectra for the BODIPY band, which appeared around λ_{abs} = 500 nm for both compounds, whereas the coumarin band displayed shifts of up to $\Delta\lambda$ = 12–13 nm depending on the solvent.

Regarding the emission spectra in different solvents, the emission from the BODIPY core was also found to be polarity-independent both under irradiation at λ_{exc} = 440 nm (Fig. 6) and λ_{exc} = 490 nm (ESI,‡ Fig. S15), displaying an emission fixed around λ_{em} = 520 nm regardless of the solvent. This observation confirms the success of the current approach in solving the polarity-dependence of the BODIPY emission, which was one of the main objectives of this work. Nonetheless, paralleling our above observations on the absorption spectra, the emission

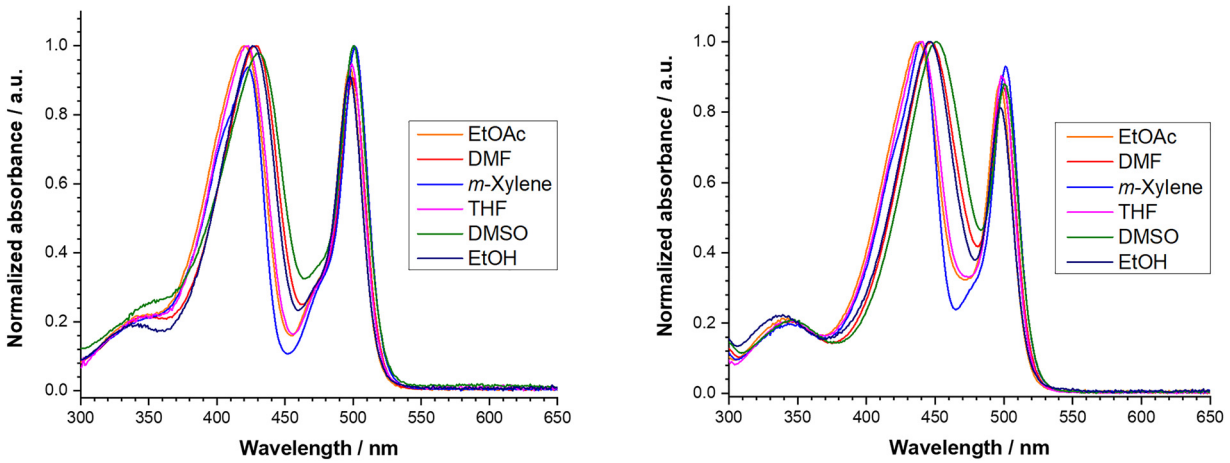

Fig. 5 Optical absorption and for **FMR-I** (left) and **FMR-II** (right) in different solvents at 10^{-5} M.

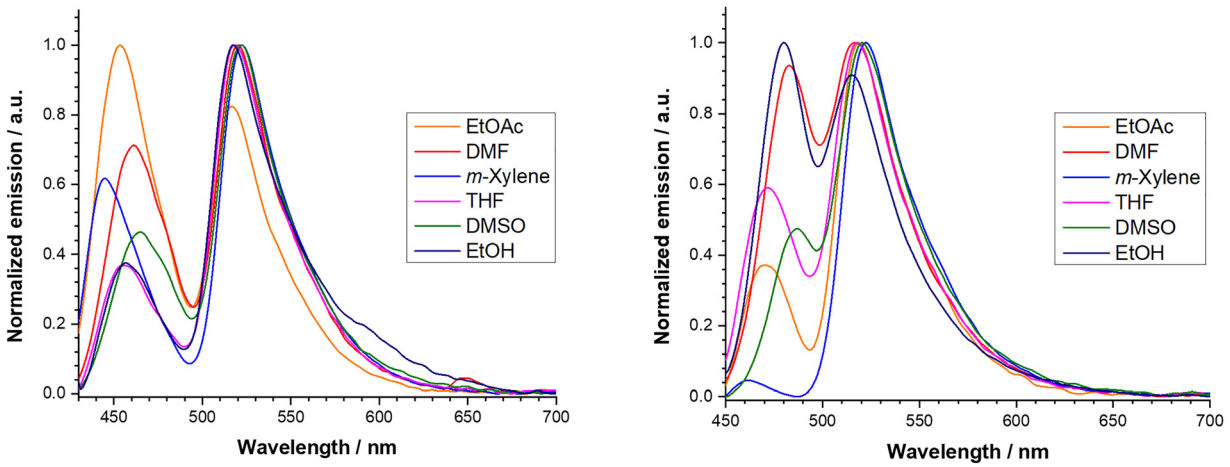

Fig. 6 Emission spectra for **FMR-I** (left) and **FMR-II** (right) in different solvents at 10^{-5} M, under excitation at λ_{exc} = 440 nm.

from the coumarin fragment was more complex, with noticeable changes in intensity and wavelength for both **FMR-I** and **FMR-II**. This phenomenon can potentially be accounted to the push–pull architecture of the coumarin fragment, which as discussed earlier, imparts a charge transfer nature to its lowest-lying vertical excitation. Upon irradiation, the resulting charge-separated species would become more stabilized in polar solvents and thus emission from the coumarin becomes affected by polarity. Additionally the viscosity (η) of the solvents (η = 0.284 to 1.074 cP)[41] was also considered as a potential physicochemical parameter that could affect the emission of the coumarin, analogous to structurally-related julolidine-based FMRs.[42] The response in any case seems complex, with none of these variables playing a dominant role in the observed response, with no clear tendencies observed in plots of the relative fluorescence intensity of the coumarin band *vs.* the ε and η values of the solvents (ESI,‡ Fig. S16). The observation of such a complex response in these solvents required us to conduct quantitative viscosity fluorescent measurements, which are discussed in the next section.

Viscosity sensing properties

A study of the fluorescent viscosity sensing properties of the target fluorophores was undertook in the context of their potential applications as microviscosity sensors. The measurements were performed quantitatively by studying solutions of the fluorophores in DMSO/glycerol mixtures with increasing glycerol molar fractions, whose specific viscosities were calculated using the Nissan–Grunbberg model.[43,44]

Given that the viscosity of glycerol (η = 934 cP) is much higher than that of DMSO (η = 1.987 cP),[41] the experiment allows assessing the effect of the variations of viscosity on the emission of the FMRs. Conversely, both solvents have comparable dielectric constants (ε = 46.53 and 47.24 D, respectively)[41] thus precluding potential interferences from changes in polarity during these viscosity measurements.

The viscosity sensing properties of the FMRs were studied under irradiation at λ_{exc} = 420 and 440 nm for **FMR-I** and **FMR-II**, respectively. The recorded emission spectra are presented in Fig. 7, where the emission properties are clearly modified over the whole range of viscosities (η = 2 to 377 cP). As it can be seen,

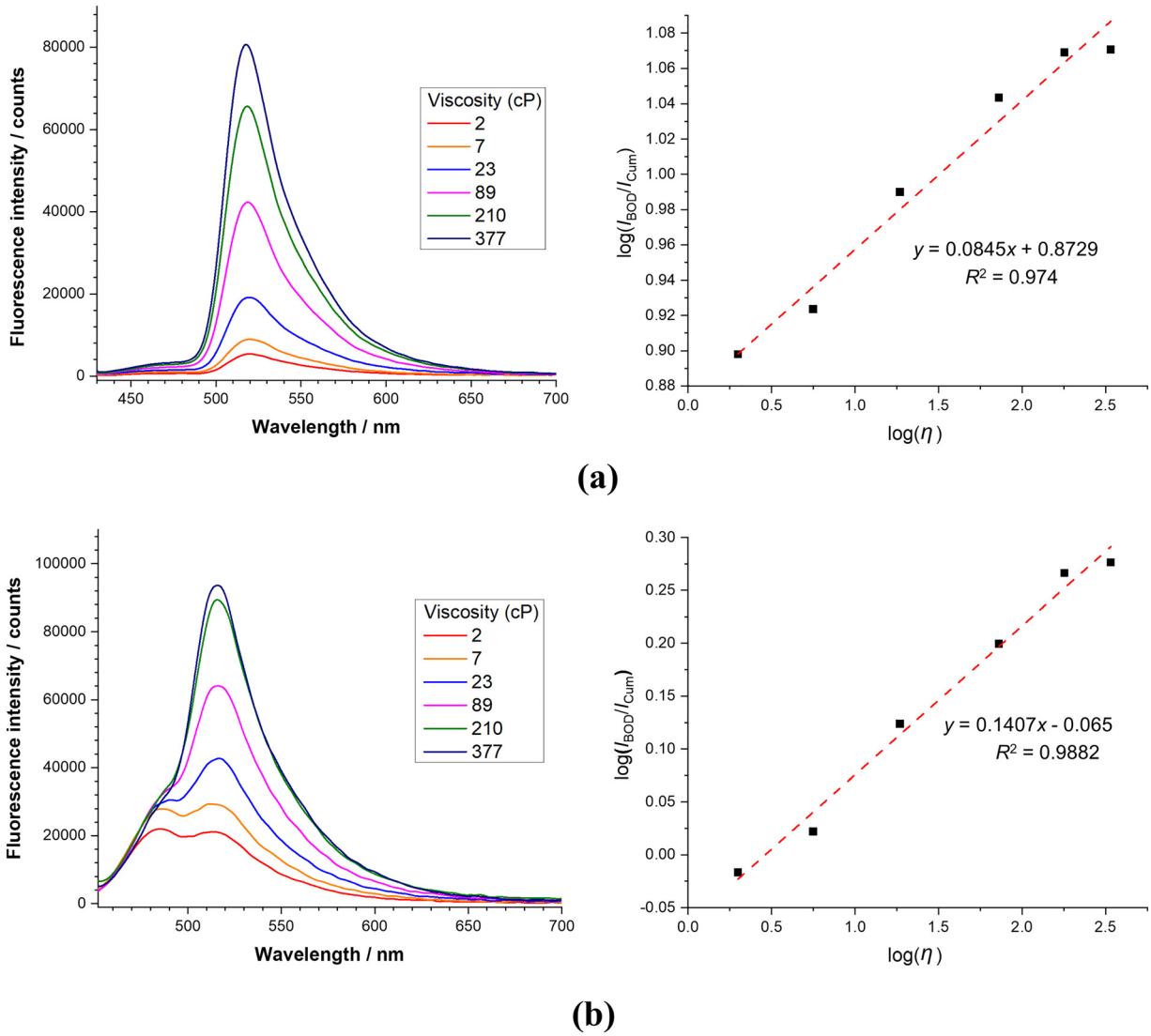

Fig. 7 Variation of the emission spectra with changes of viscosity in DMSO/glycerol mixtures for (a) **FMR-I** (λ_{exc} = 420 nm) and (b) **FMR-II** (λ_{exc} = 440 nm). Linear fits (discontinuous red lines) from double-logarithmic plots of the ratio of the fluorescent intensity of the BODIPY and coumarin bands (I_{BOD}/I_{Cum}) as functions of the viscosity are also presented, using viscosity values (η = 2 to 377 cP) calculated through the Nissan–Grunbberg model.[43,44]

the emission from the BODIPY fluorophore, centered around λ_{em} = 519 and 514 nm for **FMR-I** and **FMR-II**, respectively, becomes remarkedly more intense as the viscosity increases, while changes in the emission intensity from the coumarin fragment, centered around λ_{em} = 466 and 484 nm, respectively, are comparatively much less important. Ratiometric analyses of the observed fluorescent responses gratifyingly displayed a double-logarithmic relationship between the ratio of the fluorescence intensity of the BODIPY and coumarin bands (I_{BOD}/I_{Cum}) and the viscosity, in good agreement with the Förster–Hofmann theory.[45,46] Linear fits of the double-logarithmic plots showed good correlation coefficients, with R^2 = 0.974 and R^2 = 0.988 for **FMR-I** and **FMR-II**, respectively, thus demonstrating the excellent capabilities of the developed FMRs for accurately signaling viscosity changes over a broad interval of viscosities.

At this stage of the study, it is pertinent to compare the capabilities of the **FRM-I** and **FRM-II** probes with some analogs reported in the literature, in order to highlight both their strengths and the areas for improvement in their design. It is important to emphasize that the molecular sensors presented here exhibit a novel structural design that overcomes certain limitations previously observed in FMRs based on BODIPYs and coumarins. Although these earlier systems have proven useful for detecting local microviscosities, their dynamic range is generally restricted to low-viscosity environments.[22] In contrast, **FRM-I** and **FRM-II**, being non-conjugated bichromophoric compounds, extend their efficacy as ratiometric sensors to medium and high viscosity ranges, thus broadening their applicability in cellular microviscosity studies.

Among other relevant molecular rotors are BODIPY-estradiol derivatives,[47] which were designed to enhance uptake in cancer

cell lines through functionalization with molecular fragments recognizable by cellular structures, such as amino acids,[48] carbohydrates,[49] and lipids.[50] Although the compounds in this study have not been biologically evaluated, the incorporation of a coumarin fragment in **FMR-I** and **FMR-II** represents a distinctive feature with potential therapeutic value. Coumarins are known for their antibacterial[51] and antitumor[52] activities, and several of their derivatives have shown inhibition of carbonic anhydrase,[53] an enzyme involved in tumor progression. This suggests that the presence of this scaffold could add diagnostic and therapeutic value to the sensors, particularly in oncological contexts.

Finally, conjugated BODIPY-fluorene rotors have proven to be effective ratiometric sensors,[54] exhibiting minimal sensitivity to solvent polarity. This property is most likely due to the absence of a push–pull system in the fluorene scaffold. In this regard, a structural improvement opportunity lies in modifying the amino group on the coumarin, which could further reduce its sensitivity to polarity and bring its behavior closer to that of an ideal ratiometric sensor.

The evolution of these sensors toward optimized versions has the potential to open new opportunities in bioimaging and molecular diagnostics. Their remarkable structural versatility represents an ideal starting point for the development of advanced directed functionalization strategies. In particular, if their biological activity is confirmed, **FMR-I** and **FMR-II** could emerge as promising candidates for specific clinical applications. Furthermore, these molecules could be compared with new synthetic analogs incorporating a BF_2 moiety instead of the BPh_2 in the present investigation, which would significantly enhance their fluorescence. Our research group is currently undertaking research efforts toward investigating these interesting opportunities.

Conclusion

This work presents a study on two fluorescent molecular rotors (FMRs) designed as ratiometric viscosity sensors. The structure of the target molecules contained two different fluorophores, *i.e.* an amino-coumarin derivative and a boron-dipyrromethane (BODIPY) dye. Our molecular engineering strategy towards these ratiometric viscosity sensors involved using the BODIPY fragment as the viscosity-sensitive fluorophore, while the amino-coumarin would function as a reference fluorophore. Our study tackles a problematic from a previous report by our research group[22] in which albeit efficiently functioning as ratiometric viscosity sensors, similar coumarin/BODIPY dyads displayed a deleterious influence of polarity on the emission from the BODIPY fragment, thus interfering with the analytical response of the probes. Our strategy to solve this issue was to disrupt the conjugation between both fluorophores, thus electronically isolating the viscosity-sensitive BODIPY fluorophore from the coumarin fragment, which due to the presence of a clear push–pull architecture, displays an important charge-transfer character for its lowest-lying electronic excitations.

Detailed structural and electronic structure analyses, with support from SXRD data and DFT computations, revealed the successful isolation of both submolecular fragments, which gratifyingly resulted in the pursued polarity-independent emission from the BODIPY fluorophore, leading to excellent ratiometric fluorescent responses for both **FMR-I** and **FMR-II**, as revealed through Förster–Hofmann logarithmic analyses. Further optimization of the molecular structure may involve replacing the ester group for another bridge, as the ester bridge acts as an electron withdrawing group that together with the strong electron-donating capabilities of the amino group, imparts an important push–pull character to the coumarin fragment, which may favour the population of nonradiative intramolecular charge transfer states, thus potentially contributing to the low fluorescence of the current FMRs. Nonetheless, the results presented herein pave the way for applications of the developed FMRs as advanced tools for measuring changes in microviscosity, which is a rapidly-evolving research domain that currently attracts significant research interest, due to the usefulness of ratiometric fluorescent sensors in the rapid and accurate diagnosis of diverse diseases.

Experimental section

Materials and equipment

All reagents were commercially available and used without further purification. Reagent-grade solvents were purified by distillation over drying agents. Reactions were monitored by analytical thin layer chromatography (TLC) on pre-coated silica gel plates (ALUGRAM SIL G/UV254), under UV light. Column chromatography was performed on silica gel (230–400 mesh) employing an appropriate eluent.[55] HRMS data were acquired using a LC–MS Orbitrap Thermo Fisher Scientific spectrometer. Absorption and fluorescence spectra were acquired using Thermo Scientific Evolution 220 and PerkinElmer FL 6500 spectrophotometers, respectively, employing spectroscopic grade solvents. Infrared spectra were recorded on an Agilent Cary Spectrum 600 FT-IR spectrometer. Quantum yields were measured using an integrating sphere. Microwave-assisted reactions were carried out using a CEM Discover SP microwave reactor. Coumarin derivative **3a** was synthesized as described elsewhere;[56] spectroscopic data were in good agreement.

NMR spectroscopy

NMR spectra were recorded using JEOL ECA 500 MHz and Bruker 400 Avance MHz spectrophotometers 298 K employing deuterated solvents and standard pulse sequences; chemical shifts for ^{1}H- and ^{13}C-NMR data are relative to the residual nondeuterated solvent signal, fixed at δ = 7.26 ppm for ^{1}H-NMR and δ = 77.00 ppm for ^{13}C-NMR. For ^{11}B-NMR, chemical shifts are reported relative to $BF_3{\cdot}OEt_2$ as an external standard. Chemical shifts are given in ppm with multiplicities abbreviated as singlet (s), doublet (d), doublet of doublets (dd), triplet (t), quartet (q), quintet (p) and multiplet (m).

X-Ray diffraction studies

Crystals of compound **FMR-I** were grown by slow evaporation of a saturated chloroform solution of the analyte. Structural data were collected on a Bruker D8 VENTURE diffractometer at 293 K. Crystals were mounted on conventional MicroLoops.™ All heavier atoms were found by difference Fourier mapping and all atoms appeared in the first solution. Hydrogen atoms were refined isotropically at calculated positions using a riding model. Reflection data were corrected for Lorentz and polarization effects. The first solution, refinement and output data were obtained using the SHELXL-2019 program.[57] Disorder of the diethylamino group and the ester bridge was modelled over two and three positions, respectively, with atomic coordinates and occupancies allowed to refine freely. All software manipulations were performed through the ShelXle program.[58] ORTEP3[59] and Mercury 2024[60] were used to prepare artwork representations. Deposition Number 2424050 contains the supplementary crystallographic data for this paper. These data are provided free of charge by the joint Cambridge Crystallographic Data Centre and Fachinformationszentrum Karlsruhe Access Structures service.

Syntheses

8-(4-hydroxyphenyl)-4,4-diphenyl-BODIPY (**2**). To a round-bottom flask containing 4-hydroxybenzaldehyde (5.00 g, 40.94 mmol) were added pyrrole (200 mL), anhydrous dichloromethane (250 mL) and trifluoroacetic acid (0.13 mL). The mixture was stirred under nitrogen for 3 hours, yielding intermediate *meso*-(4-hydroxyphenyl)-dipyrromethane,24 as a pale pink solid in 76% yield after and purification by column chromatography using a gradient of hexane and ethyl acetate (1/1) as eluent. This intermediate (0.45 g, 1.90 mmol) was dissolved in tetrahydrofuran (15 mL), treated with 2,3-dichloro-5,6-dicyano-1,4-benzoquinone (0.46 g, 2.02 mmol) and stirred for 1 hour, followed by the addition of a 0.13 M diethyl ether solution of diphenylborinic acid (15 mL). After refluxing for 10 hours, the reaction was chilled to room temperature and the solvents were removed under reduced pressure. The crude product was redissolved in dichloromethane (25 mL) and treated with brine (3 × 25 mL). The combined organic phases were dried over anhydrous Na_2SO_4 and concentrated under reduced pressure. After purification by column chromatography using a gradient of hexane and ethyl acetate (from 1/0 to 1/1) as eluent, the title compound was obtained as an orange solid in 43% yield. ^{1}H-NMR (400 MHz, $CDCl_3$) δ 7.57 (s, 2H, H-1), 7.53 (d, J = 8.6 Hz, 2H, H-7), 7.25–7.15 (m, 10H, H-2a/H-4a/H-3a), 7.00 (d, J = 4.2 Hz, 2H, H-3), 6.96 (d, J = 8.6 Hz, 2H, H-8), 6.51 (dd, J = 4.2, 1.8 Hz, 2H, H-2), 5.66 (s, 1H, OH). ^{13}C-NMR δ ($CDCl_3$, 100 MHz): 157.83 (C-9), 146.73 (C-5), 144.53 (C-1), 134.56 (C-4), 132.73 (C-3a), 132.47 (C-7), 128.89 (C-3), 127.31 (C-2a), 127.12 (C-6), 126.08 (C-4a), 117.20 (C-2), 115.24 (C-8) (signal for C-1a not observed). ^{11}B-NMR δ ($CDCl_3$, 128 MHz): -0.49 (s, BPh_2). FT-IR (ATR, cm^{-1}): 3324 (νO-H), 1538 (νC=C), 1077 (ν_{as}B–N). HRMS (ESI-TOF$^+$) m/z: $[M + H]^+$ anal. calcd for $C_{27}H_{22}BN_2O$: 401.1825. Found: 401.1829. Error = 0.99 ppm.

Fluorescent molecular rotor I (FMR-I). To a round-bottom flask containing BODIPY **2** (0.05 g, 0.13 mmol) and 7-(diethylamino)-2-oxo-2*H*-chromene-3-carboxylic acid (3a) (0.04 g, 0.14 mmol) were added dichloromethane (15 mL), *N*,*N*′-dicyclohexylcarbodiimide (0.03 g, 0.14 mmol) and 4-dimethylaminopyridine (0.017 g, 0.14 mmol). The mixture was treated with microwave radiation (100 W) for 1 hour at 40 °C (5 °C min^{-1} gradient) and allowed to chill to room temperature. The crude product was first purified by column chromatography using a gradient of dichloromethane and methanol (from 1/0 to 9/1) as eluent. Subsequently, a second column was performed using a gradient of hexane and ethyl acetate ethyl acetate (from 1/0 to 1/1) as eluent, yielding the title compound as an orange solid in 92% yield. ^{1}H-NMR (500 MHz, $CDCl_3$) δ 8.64 (s, 1H, H-12), 7.66 (d, J = 8.6 Hz, 2H, H-7), 7.59 (t, J = 1.5 Hz, 2H, H-1), 7.43 (d, J = 9.0 Hz, 1H, H-14), 7.40 (d, J = 8.6 Hz, 2H, H-8), 7.26–7.23 (m, 4H, H-2a), 7.22–7.17 (m, 6H, H-4a/H-3a), 7.00 (dd, J = 4.3, 1.2 Hz, 4H, H-3), 6.66 (dd, J = 9.0, 2.5 Hz, 1H, H-15), 6.54–6.51 (m, 3H, H-2/H-17), 3.49 (q, J = 7.2 Hz, 4H, H-20), 1.28–1.25 (m, 6H, H-21). ^{13}C-NMR δ ($CDCl_3$, 125 MHz): 162.52 (C-10), 158.94 (C-18), 158.02 (C-16), 153.50 (C-5), 152.51 (C-9), 150.51 (C-12), 145.84 (C-19), 145.10 (C-1), 134.56 (C-4), 132.72 (C-3a), 131.95 (C-6), 131.62 (C-7), 131.53 (C-14), 129.10 (C-3), 127.36 (C-2a), 126.13 (C-4a), 121.80 (C-8), 117.56 (C-2), 109.86 (C-15), 107.83 (C-13), 107.05 (C-11), 96.77 (C-17), 45.24 (C-20), 29.69 (C-21). (Signal for C-1a not observed). ^{11}B-NMR δ ($CDCl_3$, 128 MHz): −0.54 (s, BPh_2). FT-IR (ATR, cm^{-1}): 1736 (νC=O, lactone), 1713 (νC=O, ester), 1577 (νC=C), 1184 (νC–O), 1056 (ν_{as}B–N). HRMS (ESI-TOF$^+$) m/z: $[M + H]^+$ anal. calcd for $C_{41}H_{35}BN_3O_4$: 644.2721. Found: 644.2728. Error = 2.03 ppm.

Fluorescent molecular rotor II (FMR-II). Synthesized in an analogous manner to that described above for **FMR-I**, but using coumarin 343 (**2b**) as a coupling partner. The procedure yielded the title compound as an orange solid in 88% yield. ^{1}H-NMR (500 MHz, $CDCl_3$) δ 8.54 (s, 1H, H-12), 7.67 (d, J = 8.7 Hz, 2H, H-7), 7.60 (d, J = 0.9 Hz, 2H, H-1), 7.41 (d, J = 8.8 Hz, 2H, H-8), 7.28–7.24 (m, 4H, H-2a), 7.23–7.18 (m, 6H, H-4a/H-3a), 7.03–6.99 (m, 3H, H-14/H-3), 6.58–6.50 (m, 2H, H-2), 3.38 (q, J = 6.0 Hz, 4H, H-23/H-20), 2.92 (t, J = 6.4 Hz, 2H, H-22), 2.79 (t, J = 6.3 Hz, 2H, H-25), 2.00 (p, J = 6.2 Hz, 4H, H-24/H-21). ^{13}C-NMR δ ($CDCl_3$, 125 MHz) 162.74 (C-10), 158.38 (C-18), 153.90 (C-16), 152.66 (C-9), 150.28 (C-12), 149.26 (C-19), 145.91 (C-5), 145.04 (C-1), 134.55 (C-4), 132.71 (C-3a), 131.77 (C-6), 131.55 (C-7), 129.10 (C-3), 127.33 (C-14/C-2a), 126.11 (C-4a), 121.85 (C-8), 119.52 (C-15), 117.52 (C-2), 107.69 (C-13), 105.78 (C-11), 105.39 (C-17), 50.36 (C-23), 49.97 (C-20), 27.39 (C-25), 21.05 (C-24), 20.06 (C-21), 20.02 (C-22) (signal for C-1a not observed). ^{11}B-NMR δ ($CDCl_3$, 128 MHz): −0.22 (s, BPh_2). FT-IR (ATR, cm^{-1}): 1764.76 ($\nu_{C=O}$, lactone), 1728.00 (νC=O, ester), 1519.36 (νC=C), 1164.68 (νC–O), 1055.29 (ν_{as}B–N). HRMS (ESI-TOF$^+$) m/z: $[M + H]^+$ anal. calcd for $C_{43}H_{35}BN_3O_4$: 668.2721. Found: 668.2731. Error = 1.50 ppm.

Computational methods

Quantum chemical computations were performed within the framework of the Density Functional Theory (DFT) using the

M06-2X functional combined with the double-ζ 6-31G+G(d,p) polarized basis set, through the Gaussian-09 program package.[61] The M06-2X hybrid functional was chosen on the basis of a previous report by Jacquemin and co-workers recommending this functional as the most reliable DFT approach for molecules based on BODIPY fluorophores,[62,63] and aiming at taking into account noncovalent interactions, for which *meta*-GGA functionals usually outperform many other hybrid functionals.[64,65] Solvation effects were incorporated through the LR-PCM approach.[66] Starting geometries for the monomers/dimers were built upon or obtained from the SXRD data for **FMR-I**. Unless otherwise specified, molecular structures were optimized without imposing any constraints. Alternatively, in some cases partially-constrained optimizations were performed to better represent the crystallographic conformations, with coordinates for all the H-atoms and any disordered heavier atom allowed to optimize freely in every case, while other non-disordered atoms were 'frozen' in their crystallographic positions. Analytical frequency computations showed no imaginary frequencies related to unconstrained atoms, confirming these equilibrium structures as true local minima.

TD-DFT computations were carried out on optimized geometries of **FMR-I** and **FMR-II** in DMSO at the same level of theory, taking into account vertical excitations towards the 12 lowest-lying excited states. In order to confirm or correct the NMR assignments, Gauge invariant atomic orbital (GIAO) computations of isotropic magnetic shieldings of ^{13}C nuclei were performed in chloroform. Although the methodology provides absolute chemical shifts, for clarity, they are herein reported as scaled with respect to an external tetramethylsilane (TMS) reference computed at the same level of theory. Quantum theory of atoms in molecules (QTAIM) topological analyses of the electron density gradient were carried out employing Multiwfn 3.8[67] on optimized structures. Fulfillment of the Poincaré–Hopf relationship[68] was systematically inspected. Molecular graphs were plotted using VMD 1.9.4.[69]

Data availability

The data supporting the findings of this study, including characterization data (NMR and HRMS spectra, and computational files), are provided in the ESI‡ file associated with this article. Additional data, if required, are available from the corresponding author upon reasonable request.

Conflicts of interest

The authors state that there are no conflicts to declare.

Acknowledgements

E. O. acknowledges SECIHTI for providing his doctoral scholarship (CVU 917328). N. F. acknowledges support from PAIP and PAPIIT (IN228625). P. L.-V. acknowledges SECIHTI (CVU 589363) and the Faculty of Chemistry of National Autonomous University of México (FQ-UNAM) for their economic support through a Repatriation Grant (grant number: I1200/111/2024). S. M. R.-M. thanks SECIHTI (CVU 554888) for her postdoctoral fellowship. Supercomputing resources from DGTIC-UNAM through Project "LANCAD-UNAM-DGTIC-268" are acknowledged.

References

1 D. J. Mulder, A. P. H. J. Schenning and C. W. M. Bastiaansen, *J. Mater. Chem. C*, 2014, **2**, 6695–6705.
2 G. Su, Z. Li and R. Dai, *ACS Appl. Polym. Mater.*, 2022, **4**, 3131–3152.
3 A. Concellón, D. Fong and T. M. Swager, *J. Am. Chem. Soc.*, 2021, **143**, 9177–9182.
4 A. Kisiel, K. Kłucińska, Z. Głębicka, M. Gniadek, K. Maksymiuk and A. Michalska, *Analyst*, 2014, **139**, 2515–2524.
5 R. Gui, H. Jin, X. Bu, Y. Fu, Z. Wang and Q. Liu, *Coord. Chem. Rev.*, 2019, **383**, 82–103.
6 T. Yoshihara, Y. Yamaguchi, M. Hosaka, T. Takeuchi and S. Tobita, *Angew. Chem., Int. Ed.*, 2012, **51**, 4148–4151.
7 S. Abbasi-Moayed, H. Golmohammadi, A. Bigdeli and M. R. Hormozi-Nezhad, *Analyst*, 2018, **143**, 3415–3424.
8 L. Zhu, M. Fu, B. Yin, L. Wang, Y. Chen and Q. Zhu, *Dyes Pigm.*, 2020, **172**, 107859.
9 R. J. Howard and W. H. Sawyer, *Parasitology*, 1980, **80**, 331–342.
10 D. Jurgutis, G. Jarockyte, V. Poderys, J. Dodonova-Vaitkuniene, S. Tumkevicius, A. Vysniauskas, R. Rotomskis and V. Karabanovas, *Int. J. Mol. Sci.*, 2022, **23**, 5687.
11 W. Shen, P. Wang, Z. Xie, H. Zhou, Y. Hu, M. Fu and Q. Zhu, *Talanta*, 2021, **234**, 122621.
12 C. Sumbilla and J. R. Lakowicz, *J. Neurochem.*, 1982, **38**, 1699–1708.
13 M. Kubánková, I. López-Duarte, D. Kiryushko and M. K. Kuimova, *Soft Matter*, 2018, **14**, 9466–9474.
14 M. Paez-Perez and M. K. Kuimova, *Angew. Chem., Int. Ed.*, 2024, **63**, e202311233.
15 M. A. Haidekker, T. P. Brady, D. Lichlyter and E. A. Theodorakis, *J. Am. Chem. Soc.*, 2006, **128**, 398–399.
16 D. Cao, Z. Liu, P. Verwilst, S. Koo, P. Jangjili, J. S. Kim and W. Lin, *Chem. Rev.*, 2019, **119**, 10403–10519.
17 C. E. Wheelock, *J. Am. Chem. Soc.*, 1959, **81**, 1348–1352.
18 E. K. Haralambos, *Curr. Pharm. Des.*, 2004, **10**, 3835–3852.
19 A. Loudet and K. Burgess, *Chem. Rev.*, 2007, **107**, 4891–4932.
20 N. Boens, V. Leen and W. Dehaen, *Chem. Soc. Rev.*, 2012, **41**, 1130–1172.
21 M. Poddar and R. Misra, *Coord. Chem. Rev.*, 2020, **421**, 213462.
22 J. Ordóñez-Hernández, A. Jiménez-Sánchez, H. García-Ortega, N. Sánchez-Puig, M. Flores-Álamo, R. Santillan and N. Farfán, *Dyes Pigm.*, 2018, **157**, 305–313.
23 L. Blancarte-Carrazco, S. M. Rojas-Montoya, O. González-Antonio, E. Ordaz-Romero, R. Santillan and N. Farfán, *Tetrahedron*, 2025, **172**, 134438.
24 A. N. Kursunlu, E. Guler, H. I. Ucan and R. W. Boyle, *Dyes Pigm.*, 2012, **94**, 496–502.

25 P. Labra-Vázquez, A. Galano, M. Romero-Ávila, M. Flores-Álamo and M. A. Iglesias-Arteaga, *ARKIVOC*, 2013, **iv**, 107–125.
26 P. Labra-Vázquez, A. Z. Lugo-Aranda, M. Maldonado-Domínguez, R. Arcos-Ramos, M. d P. Carreon-Castro, R. Santillan and N. Farfán, *J. Mol. Struct.*, 2015, **1101**, 116–123.
27 H. Lu, Q. Wang, L. Gai, Z. Li, Y. Deng, X. Xiao, G. Lai and Z. Shen, *Chem. – Eur. J.*, 2012, **18**, 7852–7861.
28 P. Labra-Vázquez, R. Flores-Cruz, A. Galindo-Hernández, J. Cabrera-González, C. Guzmán-Cedillo, A. Jiménez-Sánchez, P. G. Lacroix, R. Santillan, N. Farfán and R. Núñez, *Chem. – Eur. J.*, 2020, **26**, 16530–16540.
29 D. Martínez-Bourget, E. Rocha, P. Labra-Vázquez, R. Santillan, B. Ortiz-López, V. Ortiz-Navarrete, V. Maraval, R. Chauvin and N. Farfán, *Spectrochim. Acta, Part A*, 2022, **283**, 121704.
30 M. Farfán-Paredes, P. Labra-Vázquez, O. González-Antonio, D. Martínez-Bourget, C. Guzmán-Cedillo, A. Galindo-Hernández, M. Romero, R. Santillan and N. Farfán, *Chem. – Eur. J.*, 2023, **29**, e202302847.
31 Z. Wang, X. Guo, Z. Kang, Q. Wu, H. Li, C. Cheng, C. Yu, L. Jiao and E. Hao, *Org. Lett.*, 2023, **25**, 744–749.
32 R. F. W. Bader, P. J. MacDougall and C. D. H. Lau, *J. Am. Chem. Soc.*, 1984, **106**, 1594–1605.
33 R. F. W. Bader and H. Essén, *J. Chem. Phys.*, 1984, **80**, 1943–1960.
34 P. Labra-Vázquez, V. Mudrak, M. Tassé, S. Mallet-Ladeira, A. Sournia-Saquet, J.-P. Malval, P. G. Lacroix and I. Malfant, *Inorg. Chem.*, 2023, **62**, 20349–20363.
35 T. Steiner, *Crystallogr. Rev.*, 2003, **9**, 177–228.
36 C. M. Ramírez-Lozano, M. Eugenia Ochoa, P. Labra-Vázquez, N. Farfán and R. Santillan, *J. Mol. Struct.*, 2023, **1272**, 134191.
37 E. Espinosa, E. Molins and C. Lecomte, *Chem. Phys. Lett.*, 1998, **285**, 170–173.
38 J. E. Willson, D. E. Brown and E. K. Timmens, *Toxicol. Appl. Pharmacol.*, 1965, **7**, 104–112.
39 M. E. El-Khouly, O. Ito, P. M. Smith and F. D'Souza, *J. Photochem. Photobiol., C*, 2004, **5**, 79–104.
40 J. Fajer, K. M. Barkigia, D. Melamed, R. M. Sweet, H. Kurreck, J. von Gersdorff, M. Plato, H. C. Rohland, G. Elger and K. Möbius, *J. Phys. Chem.*, 1996, **100**, 14236–14239.
41 W. M. Haynes, *CRC handbook of chemistry and physics*, CRC press, 2016.
42 N. Chakraborty, A. Silswal and A. L. Koner, *Sens. Diagn.*, 2024, **3**, 585–598.
43 L. Grunberg and A. H. Nissan, *Nature*, 1949, **164**, 799–800.
44 G. Angulo, M. Brucka, M. Gerecke, G. Grampp, D. Jeannerat, J. Milkiewicz, Y. Mitrev, C. Radzewicz, A. Rosspeintner, E. Vauthey and P. Wnuk, *Phys. Chem. Chem. Phys.*, 2016, **18**, 18460–18469.
45 M. K. Kuimova, *Phys. Chem. Chem. Phys.*, 2012, **14**, 12671–12686.
46 M. Ren, K. Zhou, L. Wang, K. Liu and W. Lin, *Sens. Actuators, B*, 2018, **262**, 452–459.
47 D. Martínez-Bourget, E. Rocha, P. Labra-Vázquez, R. Santillan, B. Ortiz-López, V. Ortiz-Navarrete, V. Maraval, R. Chauvin and N. Farfán, *Spectrochim. Acta, Part A*, 2022, **283**, 121704.
48 L. Mendive-Tapia, R. Subiros-Funosas, C. Zhao, F. Albericio, N. D. Read and R. Lavilla, *et al.*, *Nat. Protoc.*, 2017, **12**(8), 1588–1619.
49 P. E. Kesavan, V. Pandey, M. K. Raza, S. Mori and I. Gupta, *Bioorg. Chem.*, 2019, **91**, 103139.
50 I. A. Boldyrev, X. Zhai, M. M. Momsen, H. L. Brockman, R. E. Brown and J. G. Molotkovsky, *J. Lipid Res.*, 2007, **48**(7), 1518–1532.
51 H. L. Qin, Z. W. Zhang, L. Ravindar and K. P. Rakesh, *Eur. J. Med. Chem.*, 2020, **207**, 112832.
52 A. Rawat and A. V. B. Reddy, *Eur. J. Med. Chem. Rep.*, 2022, **5**, 100038.
53 Y. Wu, J. Xu, Y. Liu, Y. Zeng and G. Wu, *Front. Oncol.*, 2020, **10**, 592853.
54 E. Xochitiotzi-Flores, A. Jiménez-Sánchez, H. Garcia-Ortega, N. Sánchez-Puig, M. Romero-Ávila, R. Santillan and N. Farfán, *New J. Chem.*, 2016, **40**(5), 4500–4512.
55 W. C. Still, M. Kahn and A. Mitra, *J. Org. Chem.*, 1978, **43**, 2923–2925.
56 S. H. Kim, Y. Sun, J. A. Kaplan, M. W. Grinstaff and J. R. Parquette, *New J. Chem.*, 2015, **39**, 3225–3228.
57 G. Sheldrick, *Acta Crystallogr., Sect. A: Found. Adv.*, 2008, **64**, 112–122.
58 C. B. Hubschle, G. M. Sheldrick and B. Dittrich, *J. Appl. Crystallogr.*, 2011, **44**, 1281–1284.
59 L. Farrugia, *J. Appl. Crystallogr.*, 2012, **45**, 849–854.
60 C. F. Macrae, I. Sovago, S. J. Cottrell, P. T. A. Galek, P. McCabe, E. Pidcock, M. Platings, G. P. Shields, J. S. Stevens, M. Towler and P. A. Wood, *J. Appl. Crystallogr.*, 2020, **53**, 226–235.
61 M. J. Frisch, G. W. Trucks, H. B. Schlegel, G. E. Scuseria, M. A. Robb, J. R. Cheeseman, G. Scalmani, V. Barone, B. Mennucci, G. A. Petersson, H. Nakatsuji, M. Caricato, X. Li, H. P. Hratchian, A. F. Izmaylov, J. Bloino, G. Zheng, J. L. Sonnenberg, M. Hada, M. Ehara, K. Toyota, R. Fukuda, J. Hasegawa, M. Ishida, T. Nakajima, Y. Honda, O. Kitao, H. Nakai, T. Vreven, J. A. Montgomery, Jr., J. E. Peralta, F. Ogliaro, M. Bearpark, J. J. Heyd, E. Brothers, K. N. Kudin, V. N. Staroverov, T. Keith, R. Kobayashi, J. Normand, K. Raghavachari, A. Rendell, J. C. Burant, S. S. Iyengar, J. Tomasi, M. Cossi, N. Rega, J. M. Millam, M. Klene, J. E. Knox, J. B. Cross, V. Bakken, C. Adamo, J. Jaramillo, R. Gomperts, R. E. Stratmann, O. Yazyev, A. J. Austin, R. Cammi, C. Pomelli, J. W. Ochterski, R. L. Martin, K. Morokuma, V. G. Zakrzewski, G. A. Voth, P. Salvador, J. J. Dannenberg, S. Dapprich, A. D. Daniels, O. Farkas, J. B. Foresman, J. V. Ortiz, J. Cioslowski and D. J. Fox, *Gaussian 09, Revision D.01*, Gaussian, Inc., Wallingford CT, 2013.
62 A. Charaf-Eddin, B. Le Guennic and D. Jacquemin, *RSC Adv.*, 2014, **4**, 49449–49456.
63 S. Chibani, B. Le Guennic, A. Charaf-Eddin, A. D. Laurent and D. Jacquemin, *Chem. Sci.*, 2013, **4**, 1950–1963.
64 Y. Zhao and D. G. Truhlar, *Theor. Chem. Acc.*, 2008, **120**, 215–241.

65 P. Labra-Vázquez, M. E. Ochoa, L. A. Alfonso-Herrera, M. A. Vera, N. Farfán and R. Santillan, *Eur. J. Org. Chem.*, 2022, e202200351.
66 J. Tomasi, B. Mennucci and R. Cammi, *Chem. Rev.*, 2005, **105**, 2999–3094.
67 T. Lu and F. Chen, *J. Comput. Chem.*, 2012, **33**, 580–592.
68 C. F. Matta and R. J. Boyd, *The quantum theory of atoms in molecules*, 2007, pp. 1–34.
69 W. Humphrey, A. Dalke and K. Schulten, *J. Mol. Graphics*, 1996, **14**, 33–38.

